A Dynamic Model and Control Method for a Two-axis Inertially Stabilized Platform

Fei Dong, Xusheng Lei, and Wusheng Chou

***Abstract*—To realize high performance control for a two-axis inertially stabilized platform (ISP), a nonlinear dynamic model based on the geographic coordinate and a compound control method based on the back-stepping sliding mode control and adaptive radial basis function neural network (RBFNN) are proposed. Compared with traditional dynamic model based on the inertial coordinate, the nonlinear dynamic model based on the geographic coordinate constructs the direct relationship among the control inputs and criteria of the ISP. Moreover, the back-stepping sliding mode control method is proposed to handle the system nonlinearity, parameter variations and disturbances. Furthermore, the adaptive RBFNN is constructed and optimized to estimate the upper bound of the residual error on line to reduce chatting phenomenon. The asymptotic stability of the proposed control method has been proven by the Lyapunov stability theory. The effectiveness of the proposed method is validated by a series of simulations and flight tests.**

***Index Terms*—Adaptive RBFNN, Back-stepping, Inertially stabilized platform, Sliding mode, Disturbances.**

I. INTRODUCTION

THE unmanned helicopter with optical imaging sensors has become a new trend for power sector to locate faults for high voltage line. It can save costs and reduce system risks effectively [1]. However, the unmanned helicopter cannot generate ideal trajectories as planned due to wind disturbances in flight tasks [2]. Therefore, there exist certain non-ideal angle disturbances for the line of sight (LOS) of the optical imaging sensors. Thus, the photo quality degrades largely.

As a middle mechanism between the optical imaging sensors and the unmanned helicopter, the ISP can adjust the gimbals to isolate the non-ideal angle disturbances for the LOS of optical sensors [3]. However, there exists strong coupling phenomenon among the unmanned helicopter, the pitch gimbal, and the yaw gimbal of the ISP system. Furthermore, there exist multi disturbances, including the outer disturbances generated by the wind disturbances and carrier vibrations, the inner disturbances generated by mass imbalance torque, friction force and sensors measurement error [4], [5]. Consequently, the ISP with imaging payloads is a typical nonlinear and time-varying system with parameter perturbations and disturbances [6], [7]. PID control, robust control, back-stepping control, sliding mode control and neural network (NN) have been proposed to improve the control performance of the ISP system [8].

With a simple control structure, the PID controller and its deformations have become the most popular controller in practical application [9]. Zhang proposed a fuzzy-PID control method to realize stable control [10]. However, the control performance is easily affected by disturbances. The robust control can deal with system disturbances and parameter variations effectively. By choosing the controller to make the system sensitivity function to be a minimum number, Martin designed a H_∞ control method to realize stable control [11]. However, the H_∞ control methods have a conservative characteristic that the control performance will be decreased with the increment of the system robustness. With a step-by-step recursive process, the back-stepping control method can deal with the system nonlinearity effectively [12]. Peyman proposed a back-stepping control law to stabilize the LOS of a boat-board camera [13]. However the parameter variations and disturbances may weaken the control performance [14]. To improve the control performance, the efforts to combine back-stepping control and sliding mode control have been done in many studies [15]. Based on the switching control law, sliding mode control can drive the system state from any initial state to a user-specified surface to maintain the current state for all subsequent time [16]. However, a severe problem of sliding mode control is the high-frequency chattering phenomenon caused by the large gain of the switching function. The neural network (NN) can deal with system nonlinear disturbances effectively for its universal approximation ability [17], [18]. But it needs a lot of training time and sample data to optimize the NN. Since the working condition of ISP is very complex, it is hard to obtain enough sample data. Using the sliding mode control and adaptive RBFNN, Lei proposed a composite control method based on the sliding mode control and adaptive RBFNN for a three-axis

Manuscript received February 20, 2016; revised May 18, 2016 and June 24, 2016; accepted July 16, 2016. This work was supported in part by the National Basic Research Program of China under Grant 2013CB035503, by the National Natural Science Foundation of China under Grant 61273033, 61473019, 61573040, by the Beijing Science and Technology Plan under Grant D161100005816001.

F. Dong is with the School of Instrument Science and Opto-electronic Engineering, Beihang University, Beijing 100191, China (e-mail: dongfei91@126.com).

W. S. Chou is with the Robotic Institute, Beihang University, Beijing 100191, China (e-mail: wschou@buaa.edu.cn).

X. S. Lei is with the School of Instrument Science and Opto-electronic Engineering, Beihang University, Beijing 100191, China (phone: 86-13621318676; fax:86-10-82316813, e-mail: xushenglei@buaa.edu.cn).

ISP [19]. However, the control performance is easily affected by the choosing of the upper bound of residual approximation error.

To achieve high performance for a two-axis ISP, a nonlinear dynamic model based on the geographic coordinate is constructed. Using the criteria of the ISP as state variables, the proposed nonlinear dynamic model constructs the direct relationship among the control inputs and criteria of the ISP. Hence, it has a better control performance than the traditional dynamic model based on the inertial coordinate. And then, a compound control method based on the back-stepping sliding mode control method and adaptive RBFNN is proposed to reject parameter variations and disturbances. A complementary sliding surface is introduced to improve error transient response during the reaching phase as well as steady–state tracking precision. Furthermore, the adaptive RBFNN is proposed to estimate and eliminate the upper bound of state error to reduce chatting problem. With the Lyapunov theory, the weighting matrix and upper bound of approximation error can be updated online. Consequently, no priori training is needed.

The outline of the paper is organized as follows: In Section 2, the nonlinear and time-varying dynamic model of the ISP is constructed. In Section 3, the compound control method based on the back-stepping sliding mode control method and adaptive RBFNN is proposed to promote the control performance, and the adaptation laws are established. A series of simulations and flight experiments validate the effectiveness of the proposed control method in section 4, followed by the conclusions in section 5.

II. THE DYNAMIC MODEL OF THE ISP SYSTEM

The ISP system is 0.67 m in length, 0.17 m in width and 0.55 m in height, and its total weight is 13.5 kg. It is composed by the yaw and the pitch gimbal, shown in Fig. 1.The yaw and the pitch are the outer and the inner loop of the system respectively. The visible light cameras (a long focus camera and a short focus camera), infrared camera, ultraviolet camera, and a 3D laser scanner are mounted on the box of the pitch gimbal of the ISP system. Furthermore, a high performance POS is chosen to provide the attitude angle information of the payloads, whose pitch angle and yaw angle error are less than 0.003 degree and 0.005 degree respectively. Meanwhile, the open-loop optical fiber rate gyro, vg095m, is chosen to provide angular velocity information of the gimbals. Its constant drift is 15°/h. The rotary electric encoder DS-58-32-DF-C is introduced to provide the relative angular displacements of two gimbals, whose precision is 0.003 degree. Moreover, to reject the high frequency line vibration of vertical direction, four metal dampers with same stiffness are installed uniformly between the base and the helicopter.

The ISP system is mounted on the bottom of the unmanned helicopter. With the non-ideal angle disturbances of unmanned helicopter, the LOS of the optical imaging sensors will deviate planed angles correspondingly. Since the POS is mounted on the same base of the different optical sensors, it can provide the angle information of the LOS of the optical sensors. Based on the measured information of POS, gyros and encoders, the controller generates corresponding control signals to adjust the pitch and the yaw gimbal. Therefore, the LOS of the optical imaging sensors is adjusted correspondingly to eliminate angle errors to get precise images and video of the high-voltage wires and the electric towers.

As a complex multi gimbals system, three coordinates are introduced to the ISP system. The base plate coordinate x_b, y_b, z_b is fixed to the base plate, and the yaw coordinate x_a, y_a, z_a is fixed to the yaw gimbal. Furthermore, the pitch coordinate x_p, y_p, z_p is fixed to the pitch gimbal. The subscripts are used to show the corresponding coordinates. Between the base plate coordinate and the yaw coordinate, it has only one rotational angle θ_a about z_b. Meanwhile, between the yaw coordinate and the pitch coordinate, it has only one rotational angle θ_p about x_a. The angles, θ_a and θ_p, can be measured by two encoders.

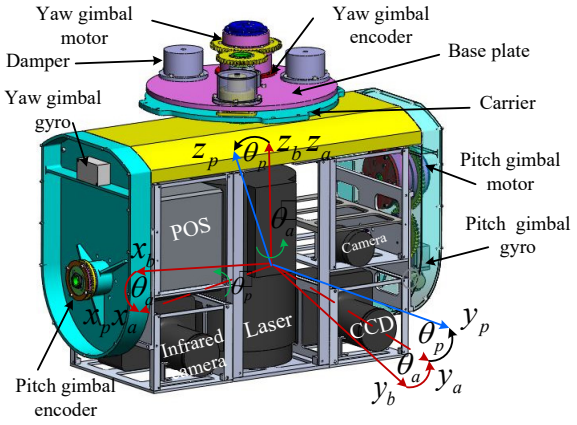

Fig. 1 Two-gimbal ISP configuration diagram

Based on the Newton Euler theory, the dynamic models of pitch gimbal and yaw gimbal can be defined as follows [9]:

$$M_{px} = J_{px}\dot{\omega}^{p}_{ipx} + (J_{pz} - J_{py})\omega^{p}_{ipy}\omega^{p}_{ipz} \tag{1}$$

$$\begin{aligned} M_{az} = {} & [J_{az}\omega^{a}_{iaz} + J_{py}\omega^{p}_{ipy}\sin\theta_p + J_{pz}\omega^{p}_{ipz}\cos\theta_p]' \\ & + (J_{ay} - J_{ax})\omega^{a}_{iax}\omega^{a}_{iay} - J_{px}\omega^{p}_{ipx}\omega^{a}_{iay} \\ & + (J_{py}\omega^{p}_{ipy}\cos\theta_p - J_{pz}\omega^{p}_{ipz}\sin\theta_p)\omega^{a}_{iax} \end{aligned} \tag{2}$$

where $\boldsymbol{M}_L = (M_{Lx}, M_{Ly}, M_{Lz})^T$ is the external torque applied on the L gimbal. $\boldsymbol{J}_L = diag(J_{Lx}, J_{Ly}, J_{Lz})$ is the moment of inertia of the L gimbal. $\boldsymbol{\omega}^{L}_{iL} = (\omega^{L}_{iLx}, \omega^{L}_{iLy}, \omega^{L}_{iLz})^T$ denotes the angular velocity of the L gimbal with respect to the inertial coordinate expressed in L gimbal coordinate. The subscript $L = p, a$ denotes the pitch and the yaw gimbal, respectively, and the subscripts x, y, z denote the components expressed in the corresponding axis of the coordinate system. The apostrophe in equation(2) means derivation.

The criteria of the ISP are the attitudes of the LOS of the optical imaging sensors, which are defined in the geographic coordinate. The attitudes of the imaging payloads with respect to geographic coordinate are defined as

$\boldsymbol{\theta}_{np}^{p}=\begin{bmatrix}\theta_{npx}^{p} & \theta_{npy}^{p} & \theta_{npz}^{p}\end{bmatrix}^{T}$, and then $\boldsymbol{\omega}_{np}^{p}=\dot{\boldsymbol{\theta}}_{np}^{p}$. Obviously, the criteria θ_{npx}^{p} and θ_{npz}^{p} are attitude angles of the pitch gimbal with respect to the geographic coordinate, which can be measured by the POS. If the angle velocities and angles of the yaw and the pitch gimbal with respect to the inertial coordinate are chosen as state variables, the angles cannot be measured directly. There exists very complex transformation from the inertial coordinate to the geographic coordinate, and transformation from the yaw gimbal coordinate to the pitch gimbal coordinate. The measurement and control performance will be lost in the computation process.

To realize high performance for a two-axis ISP, a nonlinear dynamic model based on the geographic coordinate is proposed. Since the criteria of the ISP are chosen as state variables, the error angle of LOS can be measured and eliminated directly.

Since the imaging payloads are very heavy, a torque motor mounted directly onto the gimbal axis cannot generate enough torque to realize tracking and stable control. Therefore, the DC torque motor with a gear-driven transmission is used, and its diagram is shown in Fig. 2.

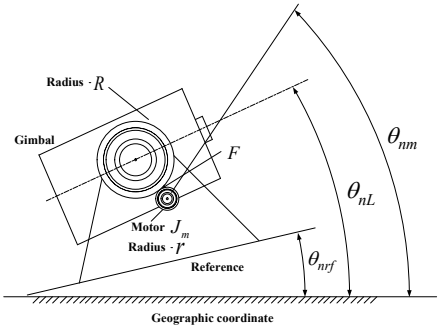

Fig. 2 A single gimbal gear-driven system

where J_m is the moment of inertia of the motor, θ_{nL}, θ_{nm} and θ_{nrf} are the attitudes of the gimbal, the corresponding motor and the reference with respect to the geographic coordinate respectively. r and R are the radii of the motor gear and the gear attached to the gimbal, F is the interacting force between the two gears. Furthermore, N is the gear ratio R/r.

The dynamic of a single gimbal gear-driven system is given by

$$\begin{cases} T_L = R_L F + T_{dL} \\ J_m \dfrac{d^2\theta_{nm}}{dt^2} = T_M - R_m F + T_{dm} \end{cases} \tag{3}$$

where T_L and T_M are the torques applied on the gimbal, and the motor respectively. T_{dL} is the disturbance torque imposed on the gimbal, which is mainly caused by mass imbalance torque. Besides, T_{dm} is the disturbance torque imposed on the motor, which is mainly caused by gearing friction torque.

The kinematic relations of the motor-gear-gimbal assembly are shown as follows:

$$\begin{cases} \theta_{nL} = \theta_{L/rf} + \theta_{nrf} \\ \theta_{nm} = \theta_{m/rf} + \theta_{nrf} \\ \theta_{m/rf} = N\theta_{L/rf} \end{cases} \tag{4}$$

where $\theta_{L/rf}$ is the relative motion of the gimbal with respect to the reference, $\theta_{m/rf}$ is the relative motion of the motor with respect to the reference. For the yaw gimbal, the reference denotes the base plate, and for the pitch gimbal, the reference denotes the yaw gimbal.

Since the output of the POS is presented in the geographic coordinate, and the output of the gyroscope vg095m is presented in the inertial coordinate, the parameters coordinates should be unified.

$$\begin{cases} \boldsymbol{\omega}_{ip}^{p} = \boldsymbol{C}_{n}^{p}\boldsymbol{\omega}_{in}^{n} + \boldsymbol{\omega}_{np}^{p} \\ \boldsymbol{\omega}_{ia}^{a} = \boldsymbol{C}_{n}^{a}\boldsymbol{\omega}_{in}^{n} + \boldsymbol{\omega}_{na}^{a} \\ \boldsymbol{\omega}_{ib}^{b} = \boldsymbol{C}_{n}^{b}\boldsymbol{\omega}_{in}^{n} + \boldsymbol{\omega}_{nb}^{b} \end{cases} \tag{5}$$

where $\boldsymbol{\omega}_{in}^{n}=(\omega_{inx}^{n},\omega_{iny}^{n},\omega_{inz}^{n})^{T}$ denotes the angular velocity of the geographic coordinate with respect to the inertial coordinate expressed in the geographic coordinate, $\boldsymbol{\omega}_{ib}^{b}=(\omega_{ibx}^{b},\omega_{iby}^{b},\omega_{ibz}^{b})^{T}$ denotes the angular velocity of the base plate coordinate with respect to the inertial coordinate expressed in the base plate coordinate, $\boldsymbol{\omega}_{n\beta}^{\beta}=(\omega_{n\beta x}^{\beta},\omega_{n\beta y}^{\beta},\omega_{n\beta z}^{\beta})^{T}$ denotes the angular velocity of the β coordinate with respect to the geographic coordinate expressed in the β coordinate, $\boldsymbol{C}_{n}^{\beta}$ denote the transformation matrix from the geographic coordinate to the β coordinate, $\beta=p,a,b$ denotes the pitch, the yaw, the base plate coordinate. Since $\boldsymbol{\omega}_{in}^{n}$ is very small, so $\boldsymbol{\omega}_{ip}^{p}\approx\boldsymbol{\omega}_{np}^{p}$, $\boldsymbol{\omega}_{ia}^{a}\approx\boldsymbol{\omega}_{na}^{a}$, $\boldsymbol{\omega}_{ib}^{b}\approx\boldsymbol{\omega}_{nb}^{b}$.

Based on the equations (1-5), the dynamic model of ISP system with respect to geographic coordinate is defined as follows:

$$\begin{aligned} \dot{\omega}_{npx}^{p} = {} & \frac{K_t K_e N^2(\omega_{nax}^{p}-\omega_{npx}^{p}) + N(N-1)R_m J_m \dot{\omega}_{nax}^{p}}{J_1 R_m} \\ & -\frac{(J_{pz}-J_{py})\omega_{npy}^{p}\omega_{npz}^{p}}{J_1} + \frac{NK_t u_p}{J_1 R_m} + \frac{NT_{dm}+T_{dp}}{J_1} \end{aligned} \tag{6}$$

$$\begin{aligned} \dot{\omega}_{npz}^{p} = {} & \frac{J_{pz}\omega_{npz}^{p}(\dot{\theta}_p+\omega_{nax}^{a})\sin 2\theta_p}{2J_3} - \frac{J_2\omega_{naz}^{a}\sin\theta_p\dot{\theta}_p}{J_3} \\ & -\frac{(J_{py}\omega_{npy}^{p}\sin\theta_p)'\cos\theta_p + J_2(\omega_{nay}^{a}\sin\theta_p)'}{J_3} \\ & +\frac{K_t K_e N^2(\omega_{nbz}^{a}-\omega_{naz}^{a}) + N(N-1)R_m J_m \dot{\omega}_{nbz}^{a}}{J_3 R_m}\cos\theta_p \\ & -\frac{J_{py}\omega_{npy}^{p}\omega_{nax}^{a}\cos^2\theta_p}{J_3} + \frac{NK_t\cos\theta_p}{J_3 R_m}u_a \\ & +\frac{J_{px}\omega_{npx}^{p}-(J_{ay}-J_{ax})\omega_{nax}^{a}}{J_3}\omega_{nay}^{a}\cos\theta_p + \frac{NT_{dm}+T_{da}}{J_3}\cos\theta_p \end{aligned} \tag{7}$$

where $J_1 = J_{px} + N^2 J_m$, $J_3 = J_{az} + N^2 J_m + J_{pz}\cos^2\theta_p$. And ω_{nax}^p, ω_{nax}^a, ω_{nay}^a, ω_{npy}^p, ω_{npz}^p can be calculated by $\boldsymbol{\omega}_{nb}^b$, ω_{naz}^a, $\boldsymbol{C}_b^a$ and $\boldsymbol{C}_a^p$ .where, $\boldsymbol{C}_b^a$ represents the transformation matrix from the base plate coordinate to the yaw coordinate. $\boldsymbol{C}_a^p$ represents the transformation matrix from the yaw coordinate to the pitch coordinate. Moreover, K_t is the torque sensitivity, K_e is the back EMF constant, R_m is the motor resistance, u_L is the total voltage input applied on the motor armature.

As a complex system, the moments of inertia of the system $\boldsymbol{J}_p$ and $\boldsymbol{J}_a$ cannot be obtained exactly. Thus they are estimated by some system parameters. At the same time, the centroid of 3D laser scanner varies with time. Hence, there are parameter variations in dynamic models (6)and(7), which are represented by Δ_1 and Δ_2, respectively.

And then the dynamic model of ISP can be given as:

$$\dot{\omega}_{npx}^p = f_1(t) + b_1 u_1 + g_1 d_1 \tag{8}$$

$$\dot{\omega}_{npz}^p = f_2(t) + b_2 u_2 + g_2 d_2 \tag{9}$$

where

$$f_1 = \frac{K_t K_e N^2(\omega_{nax}^p - \omega_{npx}^p) + N(N-1)R_m J_m \dot{\omega}_{nax}^p}{J_1 R_m} - \frac{(J_{pz} - J_{py})\omega_{npy}^p \omega_{npz}^p}{J_1},$$

$$b_1 = \frac{NK_t}{J_1 R_m}, u_1 = u_p, g_1 = \frac{1}{J_1}, \ d_1 = NT_{dm} + T_{dp} + \Delta_1,$$

$$f_2 = \frac{J_{pz}\omega_{npz}^p(\dot{\theta}_p + \omega_{nax}^a)\sin 2\theta_p}{2J_3} - \frac{J_2 \omega_{naz}^a \sin\theta_p \dot{\theta}_p}{J_3} - \frac{(J_{py}\omega_{npy}^p \sin\theta_p)'\cos\theta_p + J_2(\omega_{nay}^a \sin\theta_p)'}{J_3} + \frac{K_t K_e N^2(\omega_{nbz}^a - \omega_{naz}^a) + N(N-1)R_m J_m \dot{\omega}_{nbz}^a}{J_3 R_m}\cos\theta_p + \frac{J_{px}\omega_{npx}^p - (J_{ay} - J_{ax})\omega_{nax}^a}{J_3}\omega_{nay}^a \cos\theta_p - \frac{J_{py}\omega_{npy}^p \omega_{nax}^a \cos^2\theta_p}{J_3},$$

$$b_2 = \frac{NK_t \cos\theta_p}{J_3 R_m}, \ u_2 = u_a, \ g_2 = \frac{\cos\theta_p}{J_3}, d_2 = NT_{dm} + T_{da} + \Delta_2$$

III. THE CONTROL SYSTEM OF THE ISP SYSTEM

Since the functions $f_i, i = 1,2$ are nonlinear and time variant functions, and there exist measurement errors and unknown disturbances, it is hard to generate suitable control commands to realize high performance control. To estimate and adjust the LOS of imaging payloads to track the desired angles, a compound control method based on the back-stepping sliding mode control and adaptive RBFNN is proposed.

The block diagram of the proposed control algorithm is shown in Fig. 3. It is noted that the LOS control of the imaging payloads is divided into the pitch channel and the yaw channel. And each channel includes an attitude angle loop and an angular velocity loop respectively.

The pitch channel and the yaw channel are represented as

$$\begin{cases} \dot{x}_1 = x_2 \\ \dot{x}_2 = f_1(t) + b_1 u_1 + g_1 d_1 \\ \dot{x}_3 = x_4 \\ \dot{x}_4 = f_2(t) + b_2 u_2 + g_2 d_2 \end{cases} \tag{10}$$

where $x_1 = \theta_{npx}^p$, $x_2 = \omega_{npx}^p$, $x_3 = \theta_{npz}^p$, $x_4 = \omega_{npz}^p$.

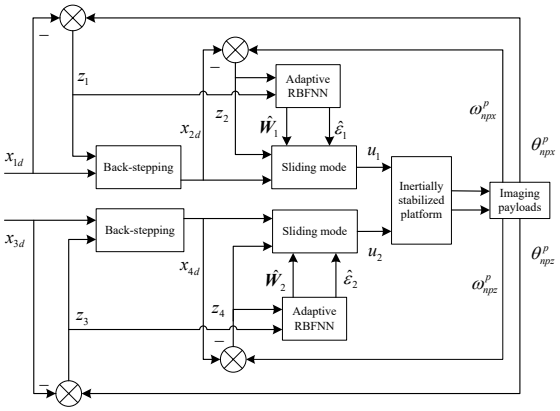

Fig. 3 The control block diagram of the proposed control method

The aim of the control method is to design suitable virtual control laws x_{2d} and x_{4d} in attitude angle loop and actual control laws u_1 and u_2 in angular velocity loop by the back stepping sliding mode control method. And then the attitude angle of the imaging payloads x_1 and x_3 can accurately track the desired attitude angle x_{1d} and x_{3d}.

Since the pitch and the yaw gimbal have similar control process, the pitch gimbal is described step-by-step to show the control process.

Step 1. Define the state error as

$$z_1 = x_1 - x_{1d} \tag{11}$$

$$z_2 = x_2 - x_{2d} \tag{12}$$

And the derivative of z_1 is obtained by

$$\dot{z}_1 = x_2 - \dot{x}_{1d} \tag{13}$$

Define the virtual control law as

$$x_{2d} = -k_1 z_1 + \dot{x}_{1d}, \tag{14}$$

where k_1 is a positive constant.

The first Lyapunov function is chosen as

$$V_1 = \frac{1}{2}z_1^2 \tag{15}$$

Differentiate V_1 with respect to time, and then

$$\dot{V}_1 = z_1\dot{z}_1 = z_1(x_2 - \dot{x}_{1d}) = z_1(x_2 - x_{2d} - k_1 z_1) = z_1 z_2 - k_1 z_1^2 \tag{16}$$

If the state error z_2 converges to zero, z_1 is asymptotically stable, so that x_1 can asymptotically track the desired attitude angle x_{1d}.

To make the state error of angular velocity loop z_2 converge to zero, the actual control law u_1 should be properly designed to dispel parameter uncertainty and disturbances.

According to the equations(10) and(12), the differentiation of $\dot{z}_2$ is obtained as

$$\dot{z}_2 = f_1(t) + b_1 u_1 + g_1 d_1 - \dot{x}_{2d} \tag{17}$$

Based on the Lyapunov function, u_1 can be directly given as

$$u_1 = -\frac{f_1(t) + g_1 d_1 - \dot{x}_{2d} + k_b z_2}{b_1} \tag{18}$$

where k_b is a positive constant.

Since the disturbances $g_1 d_1$ cannot be calculated precisely, the control performance will be decreased with the fluctuation of the disturbance value.

Step 2. The sliding mode control has high robustness against system parameter variations and external disturbances. To improve the response speed and steady-state tracking precision, the complementary sliding surface is introduced to design the actual control law u_1.

The conventional sliding surface and the complementary sliding mode are designed as follows:

$$s = z_2 + k_2 \int z_2 \, \mathrm{d}\tau \tag{19}$$

$$s_c = z_2 - k_2 \int z_2 \, \mathrm{d}\tau \tag{20}$$

where $k_2 > 0$ is the parameter decides the bandwidth of the state error s.

The relationship between s and s_c can be obtained as

$$\dot{s}_c + k_2(s + s_c) = \dot{s} \tag{21}$$

Differentiating the equation (19) with respect to time, and using

$$\dot{s} = \dot{z}_2 + k_2 z_2 = k_2 z_2 + f_1(t) + b_1 u_1 + g_1 d_1 - \dot{x}_{2d} \tag{22}$$

Then the control law u_1 can be designed as

$$u_1 = -\frac{f_1(t) + \delta \operatorname{sgn}(s + s_c) - \dot{x}_{2d} + k_2 z_2 + k_2 s}{b_1} \tag{23}$$

where $\delta \geq | g_1 d_1 |$.

Considering the second Lyapunov function as

$$V_2 = \frac{1}{2} s^2 + \frac{1}{2} s_c^2 \tag{24}$$

Differentiate V_1 with respect to time, and then

$$\begin{aligned} \dot{V}_2 &= s\dot{s} + s_c \dot{s}_c = (s + s_c)(\dot{s} - k_2 s_c) \\ &= (s + s_c)(k_2 z_2 + f_1(t) + b_1 u_1 + g_1 d_1 - \dot{x}_{2d} - k_2 s_c) \\ &= (s + s_c)(-k_2 s - k_2 s_c) = -k_2 (s + s_c)^2 \leq 0 \end{aligned} \tag{25}$$

With the increment of the system parameter variation and disturbances in the angular velocity loop, δ will be a large value, and then it will inevitably result in severe chatting problem for the switching action of $\delta \operatorname{sgn}(s + s_c)$.

Step 3. To reduce chatting phenomenon and improve the control performance, an adaptive RBFNN is introduced to approximate $g_1 d_1$ on line. With its universal approximation capabilities, the RBFNN with a finite number of hidden neurons can approximate a nonlinear function as accurate as possible.

Thereby, $g_1 d_1$ can be expressed as

$$g_1 d_1 = \boldsymbol{W}_1^{*T} \cdot \boldsymbol{\Theta}_1(z) + \varepsilon_1 \tag{26}$$

where $\boldsymbol{z} = \begin{bmatrix} z_1 & z_2 \end{bmatrix}^T$, $\boldsymbol{W}_1^* \in \Re^{1 \times l}$ is the ideal weight of the RBFNN, $\boldsymbol{\Theta}_1 \in \Re^{l \times 1}$ are the outputs of the radial basis function, l is the number of nodes of hidden layer, $\varepsilon_1 \in \Re$ is the approximation error of the RBFNN. For a certain number of nodes, ε_1 and $\boldsymbol{W}_1^*$ are unknown bounded constant variables. In this paper, the Gaussian function is selected as the radial basis function, then the jth component of $\boldsymbol{\Theta}_1 \in \Re^{l \times 1}$ can be described as

$$\Theta_j(z) = \exp\left(-\frac{(z - \boldsymbol{c}_j)^T (z - \boldsymbol{c}_j)}{\sigma_j^2}\right) \tag{27}$$

where $\boldsymbol{c}_j$ and σ_j^2 denote the center vector and the width of the Gaussian function.

The adaptive RBFNN back-stepping sliding mode control law is designed as

$$u_1 = -\frac{1}{b_1}(f_1(t) - \dot{x}_{2d} + k_2 z_2 + k_2 s + \hat{\boldsymbol{W}}_1^T \boldsymbol{\Theta}_1(z) + \hat{\varepsilon}_1) \tag{28}$$

where $\hat{\varepsilon}_1$ is the estimated value of ε_1.

Define the error vector between the ideal weight $\boldsymbol{W}_1^*$ and the estimated weight $\hat{\boldsymbol{W}}_1$ as

$$\tilde{\boldsymbol{W}}_1 = \hat{\boldsymbol{W}}_1 - \boldsymbol{W}_1^* \tag{29}$$

To develop the adaptation laws of $\hat{\boldsymbol{W}}_1$ and $\hat{\varepsilon}_1$ in the angular velocity loop, the third Lyapunov function is chosen as

$$V_3 = \frac{1}{2} s^2 + \frac{1}{2} s_c^2 + \frac{1}{2\gamma_1} \tilde{\boldsymbol{W}}_1^T \tilde{\boldsymbol{W}}_1 + \frac{1}{2\gamma_2} (\hat{\varepsilon}_1 - \varepsilon_1)^2 \tag{30}$$

where γ_1 and γ_2 are positive constants.

Then, the derivative of the Lyapunov function V_3 is expressed by

$$\begin{aligned} \dot{V}_3 &= s\dot{s} + s_c \dot{s}_c + \frac{1}{\gamma_1} \tilde{\boldsymbol{W}}_1^T \dot{\tilde{\boldsymbol{W}}}_1 + \frac{1}{\gamma_2} (\hat{\varepsilon}_1 - \varepsilon_1) \dot{\hat{\varepsilon}}_1 \\ &= (s + s_c)(\dot{s} - k_2 s_c) + \frac{1}{\gamma_1} \tilde{\boldsymbol{W}}_1^T \dot{\tilde{\boldsymbol{W}}}_1 + \frac{1}{\gamma_2} (\hat{\varepsilon}_1 - \varepsilon_1) \dot{\hat{\varepsilon}}_1 \\ &= (s + s_c)(k_2 z_2 + f_1(t) + b_1 u_1 + g_1 d_1 - \dot{x}_{2d} - k_2 s_c) \\ &\quad + \frac{1}{\gamma_1} \tilde{\boldsymbol{W}}_1^T \dot{\tilde{\boldsymbol{W}}}_1 + \frac{1}{\gamma_2} (\hat{\varepsilon}_1 - \varepsilon_1) \dot{\hat{\varepsilon}}_1 \\ &= (s + s_c)(g_1 d_1 - \hat{\boldsymbol{W}}_1^T \boldsymbol{\Theta}_1(z) - \hat{\varepsilon}_1) \\ &\quad + \frac{1}{\gamma_1} \tilde{\boldsymbol{W}}_1^T \dot{\tilde{\boldsymbol{W}}}_1 + \frac{1}{\gamma_2} (\hat{\varepsilon}_1 - \varepsilon_1) \dot{\hat{\varepsilon}}_1 - k_2 (s + s_c)^2 \end{aligned} \tag{31}$$

Since $\boldsymbol{W}_1^*$ is a constant, it is noted that

$$\dot{\tilde{\boldsymbol{W}}}_1 = \dot{\hat{\boldsymbol{W}}}_1 \tag{32}$$

Then the equation (31) can be rewritten as

This article has been accepted for publication in a future issue of this journal, but has not been fully edited. Content may change prior to final publication. Citation information: DOI 10.1109/TIE.2016.2608322, IEEE Transactions on Industrial Electronics

$$\begin{aligned}\dot{V}_3 &= (s+s_c)(-\tilde{\boldsymbol{W}}_1^T\boldsymbol{\Theta}_1(z)+\varepsilon_1-\hat{\varepsilon}_1)\\ &+\frac{1}{\gamma_1}\tilde{\boldsymbol{W}}_1^T\dot{\hat{\boldsymbol{W}}}_1+\frac{1}{\gamma_2}(\hat{\varepsilon}_1-\varepsilon_1)\dot{\hat{\varepsilon}}_1-(s+s_c)(k_3 s+k_2 s_c)\\ &=-(s+s_c)\tilde{\boldsymbol{W}}_1^T\boldsymbol{\Theta}_1(z)+\frac{1}{\gamma_1}\tilde{\boldsymbol{W}}_1^T\dot{\hat{\boldsymbol{W}}}_1+\frac{1}{\gamma_2}(\hat{\varepsilon}_1-\varepsilon_1)\dot{\hat{\varepsilon}}_1\\ &+(s+s_c)(\varepsilon_1-\hat{\varepsilon}_1)-k_2(s+s_c)^2\end{aligned} \tag{33}$$

Define the adaptation laws $\dot{\hat{\boldsymbol{W}}}_1$ and $\dot{\hat{\varepsilon}}_1$ as

$$\dot{\hat{\boldsymbol{W}}}_1=\gamma_1(s+s_c)\boldsymbol{\Theta}_1 \tag{34}$$

$$\dot{\hat{\varepsilon}}_1=\gamma_2(s+s_c) \tag{35}$$

where γ_1 and γ_2 are the learning rates.

And then

$$\dot{V}_3=-k_2(s+s_c)^2<0 \tag{36}$$

So the control errors will asymptotically converge to zero.

With the virtual control law x_{2d} given by(14) and the actual control law designed by(28), the attitude angle of the pitch channel is globally convergent, and the sliding surfaces $s=0$ and $s_c=0$ are reachable. Meanwhile, the attitude angle θ_{npx}^p of the pitch channel can track the desired attitude x_{1d} effectively.

IV. Simulations and Experiments

A. Simulations:

To validate the effectiveness of the proposed method, a series of comparisons of the back-stepping control, the back-stepping sliding mode control and the proposed control method have been designed. The corresponding wind disturbance, mass imbalance torque and friction torque have been added to simulate real working conditions.

Based on the recorder of the unmanned helicopter, the non-ideal attitude perturbations of the helicopter generated by the wind disturbance and turbulence have a random characteristic. The variation range of the angular speed is less than $10°/s$. Therefore, a random function is introduced to represent $\boldsymbol{\omega}_{ib}^b$.

$$\boldsymbol{\omega}_{ib\tau}^b=0.348*(\text{rand}(t)-0.5),\ \tau=x,y,z \tag{37}$$

where t is the simulate time.

For the ISP system, the total weight of the payloads is 28.9kg. To reduce system imbalance moment, a 5kg counterweight is introduced to adjust the centroid of the mass of the ISP. And the moment of the mass imbalance is less than 3mm. So T_{dL}, mainly composed by the mass imbalance, is represented by the disturbance with certain bound in the system, i.e.

$$T_{dL}=2.034\times(\text{rand}(t)-0.5),L=p,a \tag{38}$$

As the major section of T_{dm}, friction torque is a nonlinear function. Therefore, a sine function is proposed to represent T_{dm}, i.e.

$$T_{dm}=0.06\times(\sin(\omega t)+\sin(2\omega t)) \tag{39}$$

where ω is the fundamental frequency of the sine function, and the amplitude of the function represents the maximum static friction torque.

To simulate the real working conditions, a series of parameter perturbations have been added. The perturbations of moment of gimbal inertia Δ_1 and Δ_2 are set as 20 percent of the initial moment value. So $\boldsymbol{J}_p$ and $\boldsymbol{J}_a$ can be designed as

$$\begin{cases}J_{px}=0.769+0.307*(\text{rand}(t)-0.5)\\ J_{py}=0.952+0.381*(\text{rand}(t)-0.5)\\ J_{pz}=1.016+0.406*(\text{rand}(t)-0.5)\\ J_{ax}=0.975+0.390*(\text{rand}(t)-0.5)\\ J_{ay}=2.546+1.018*(\text{rand}(t)-0.5)\\ J_{az}=2.732+1.093*(\text{rand}(t)-0.5)\end{cases} \tag{40}$$

The adaptive RBFNN contains 100 nodes, and the initial weight matrices of the adaptive RBFNN are set as zero. The weight matrices of the adaptive RBFNN can be updated online by the weight adaptation laws in (34). And then the adaptive RBFNN can generate the corresponding estimation value of the upper bound of the residual error.

At first, the desired attitude angles and the initial attitude angles of the ISP are all set as zeros, and the attitude angles of pitch generated by the three control methods is shown in Fig. 4. The red solid line, blue dot line and green dash line are the corresponding trajectories generated by the proposed control method, back-stepping sliding mode control method and back-stepping control method. For the pitch gimbal, the maximum deviation from the desired attitude angle of the proposed control method is 0.0349 degree that is 17.06 percent and 28.26 percent of the values generated by the back-stepping control method and the back-stepping sliding mode control method respectively.

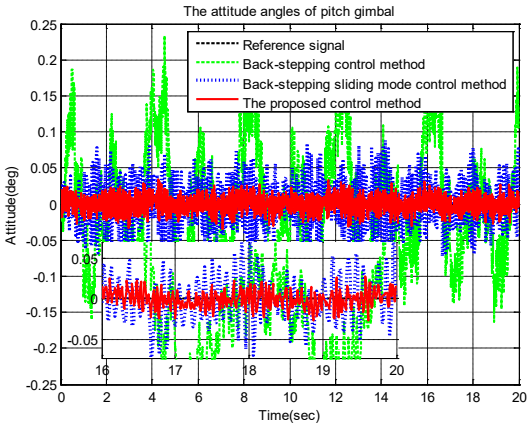

Fig. 4 The comparison of the attitude angles of pitch gimbal generated by the three control methods

Due to the nonlinearity and time variation of the ISP system, the maximum deviation of the pitch gimbal from the desired attitude angle generated by the back-stepping control method reaches to 0.2118 degree, which will affect the imaging quality of imaging payloads seriously. Since the sliding mode control method is insensitive to parameter variations and external disturbances, the back-stepping sliding mode control method

This article has been accepted for publication in a future issue of this journal, but has not been fully edited. Content may change prior to final publication. Citation information: DOI 10.1109/TIE.2016.2608322, IEEE Transactions on Industrial Electronics

achieves a better control performance than the back-stepping control method. With the adaptive RBFNN, the upper bound of the residual error can be estimated on line. Therefore, the proposed control method has a better control performance than the back-stepping sliding mode control method. Thus, the standard deviation of the proposed control method is 0.0110 degree that is 13.20 percent and 30.64 percent of values of the back-stepping control method and the back-stepping sliding mode control method.

For the yaw gimbal, the proposed control method has the best control performance. The maximum deviation and the standard deviation from the desired attitude angle are 0.0389 degree and 0.0117 degree respectively.

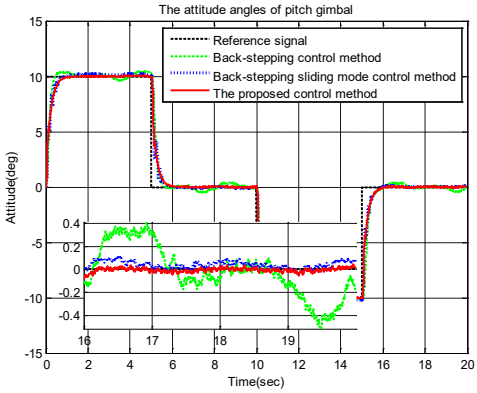

Fig. 5 The comparison of the attitude angles of pitch gimbal generated by the three control methods

To test the dynamic response characteristic, the ISP is required to make a series of angular motions of 10 degree. The initial attitude angles of the ISP are all set as zeros, the comparison of the three control methods is shown in Fig. 5. And the comparison of control performances of three methods is shown in Table I.

TABLE I
THE COMPARISON OF STABILIZATION CONTROL PERFORMANCE OF THE THREE CONTROL METHODS

	Pitch gimbal		Yaw gimbal	
	The max deviation	The standard deviation	The max deviation	The standard deviation
The back-stepping control method	0.5596	0.2373	0.5332	0.2574
The back-stepping sliding mode control method	0.1363	0.0357	0.1474	0.0396
The proposed control method	0.0945	0.0253	0.0811	0.0243

The control performance of the back-stepping control method degrades largely because of the nonlinearity, time variation and disturbances of the ISP system. The peak value of the pitch gimbal has reached to 0.56 degree and the standard deviation is 0.2373 degree. The back-stepping sliding control method and the proposed control method have a good control performance. The settling time of the proposed control method is about 0.5 second, which is similar to the back-stepping sliding mode control method. But the maximum deviation from the desired attitude angle of the pitch gimbal generated by the back-stepping sliding mode control method and the proposed control method are 0.1363 degree and 0.0945 degree. The standard deviation of the pitch gimbal generated by the proposed control method is 0.0253 degree which is 70.86 percent of the values generated by the back-stepping sliding mode control method. Consequently, the proposed control method achieves a better balance between the dynamic response speed and the stabilization precision, which meets the requirements of real application.

B. Experiments

The proposed control method has been tested on the power line inspection in Qingyuan City, Guangdong Province. The unmanned helicopter and the ISP are shown in Fig. 6. The ISP system was mounted on the bottom of the helicopter.

Fig. 6 Flight experiment system

During the flight, the ISP is required to generate the corresponding angle adjustments by the relationship between the unmanned helicopter and tower position. At the same time, the performance of the whole system was monitored by the ground real-time data processing center.

In the flight, the output attitude angles of POS were used as criteria of the control system. The corresponding attitude angles of two gimbals generated by the proposed control method in a test are shown in Fig. 7 and Fig. 8.

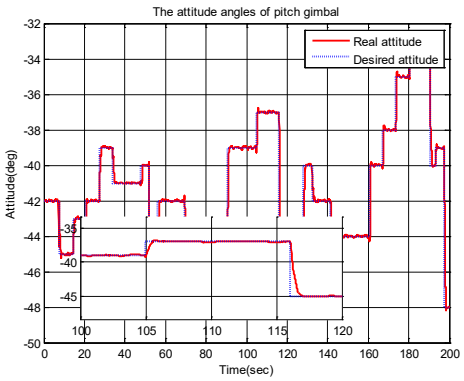

Fig. 7 The flight result of pitch gimbal with the proposed control method

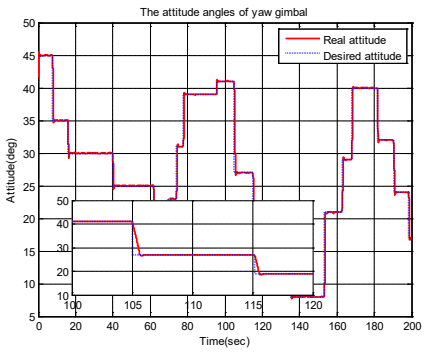

Fig. 8 The flight result of yaw gimbal with the proposed control method

The ISP realized the fast dynamic response and high precise stabilization control. The standard deviation of the pitch gimbal is 0.0414 degree and the settling time is about 0.6 second. The standard deviation of the yaw gimbal is 0.0349 degree and the settling time is about 0.5 second. The response speed of the yaw gimbal can reach 16 degree/s.

The unmanned helicopter and the ISP system have completed inspection tasks for 20 lines high-voltage wires. And the 224 faults have been located in the inspection process.

V. Conclusion

To promote the control performance of the ISP system, a nonlinear dynamic model based on the geographic coordinate and a compound control method based on the back-stepping sliding mode control and adaptive RBFNN are proposed. The ISP system has realized a fast dynamic response and high precision stabilization control performance in the high voltage line fault location experiments. The ISP system can adjust the gimbals to isolate the non-ideal attitude perturbation of imaging payloads. In the flight experiments, the standard deviation and the response speed of the ISP can achieve 0.0349 degree and 16 degree/s.

References

[1] J. M. Hilkert, "Inertially stabilized platform technology: Concepts and principles," *IEEE Contr. Syst. Mag.*, vol. 28, DOI 10.1109/MCS.2007.910256, no. 1, pp. 26-46, Feb. 2008.

[2] Z. Hurak and M. Rezac, "Image-based pointing and tracking for inertially stabilized airborne camera platform," *IEEE Trans. Contr. Syst. Technol.*, vol. 20, DOI 10.1109/TCST.2011.2164541, no. 5, pp. 1146-1159, Sept. 2012.

[3] M. K. Masten, "Inertially stabilized platform for optical imaging system: tracking dynamic targets with mobile sensors," *IEEE Contr. Syst. Mag.*, vol. 28, DOI 10.1109/MCS.2007.910201, no. 1, pp. 47-64, Feb. 2008.

[4] X. Y. Zhou, H. Y. Zhang, and R. X. Yu, "Decoupling control for two-axis inertially stabilized platform based on an inverse system and internal model control," *Mechatronics*, vol. 24, DOI 10.1016/j.mechatronics.2014.09.004, no. 8, pp. 1203–1213, Dec. 2014.

[5] J. C. Fang, R. Yin, and X. S. Lei, "An adaptive decoupling control for three-axis gyro stabilized platform based on neural networks," *Mechatronics*, vol. 27, DOI 10.1016/j.mechatronics.2015.02.002, pp. 38-46, Apr. 2015.

[6] Q. Q. Mu, G Liu, and X. S. Lei, "A RBFNN-based adaptive disturbance compensation approach applied to magnetic suspension inertially stabilized platform," *Mathematical Problems in Engineering*, vol. 2014, DOI 10.1155/2014/657985, no. 3, pp. 464-483, 2014.

[7] B. Ekstrand, "Equations of motion for a two-axes gimbal system," *IEEE Trans. Aerosp. Electron. Syst.*, vol. 37, DOI 10.1109/7.953259, no. 3, pp. 1083-1091, Jul. 2001.

[8] S. Z. Liu, C. Hong, and L. H. Sun, "Research on stabilizing and tracking control system of tracking and sighting pod," *J. of Contr. Theory and Applicat.*, vol. 10, DOI 10.1007/s11768-012-9152-8, no. 1, pp. 107-112, 2012.

[9] X. S. Lei, Y. Zou, and F. Dong, "A composite control method based on the adaptive RBFNN feedback control and the ESO for two-axis inertially stabilized platforms," *ISA Trans.*, vol. 59, DOI 10.1016/j.isatra.2015.09.011, pp. 424-433, Nov. 2015.

[10] Y. S. Zhang, T. Yang, C. Y. Li, and H. L. Sun. "Fuzzy-PID control for the position loop of aerial inertially stabilized platform," *Aerosp. Sci. Technol.*, vol. 36, DOI 10.1016/j.ast.2014.03.010, pp. 21-26, Jul. 2014.

[11] R. Martin, H. Zdenek, "Structured MIMO H∞ design for dual-stage inertial stabilization: Case study for HIFOO and Hinfstruct solvers," *Mechatronics*, vol. 23, DOI 10.1016/j.mechatronics.2013.08.003, no.8, pp. 1084–1093, Dec. 2013.

[12] Y. J. Yu, J. C. Fang, B. Xiang, and C. E. Wang. "Adaptive back-stepping tracking control for rotor shaft tilting of active magnetically suspended momentum wheel," *ISA Trans.*, vol. 53, DOI 10.1016/j.isatra.2014.07.002, no. 6, pp. 1892–1900, Nov. 2014.

[13] P. Setoodeh, A. Khayatian, and E. Farjah, "Backstepping-based control of a strapdown boatboard camera stabilizer," *Int. J. Contr. Autom. Syst.*, vol. 5, no. 1, pp. 15-23, Feb. 2007.

[14] L. D. Guo, Z. F. Tan, G. C. Li, and Q. T. Zhang, "Dynamic sliding-mode control with backstepping for stabilization loop of inertial platform," *J. Chin. Inertial Technol.*, vol. 18, no. 3, pp. 283-289, 2010.

[15] H. H. Chiang, K. C. Hsu, and I. H. Li, "Optimized adaptive motion control through an SoPC implementation for linear induction motor drives," *IEEE/ASME Trans. Mechatronics*, vol. 20, DOI 10.1109/TMECH.2014.2313594, no. 1, pp. 348-360, Feb. 2015.

[16] C. Peng, Y. Bai, X. Gong, and Y. T. Tian, "Modeling and robust backstepping sliding mode control with Adaptive RBFNN for a novel coaxial eight-rotor UAV," *IEEE/CAA J. Autom. Sinica*, vol. 2, DOI 10.1109/JAS.2015.7032906, no. 1, pp. 56-64, Jan. 2015.

[17] X. S. Lei, and P. Lu, "The adaptive radial basis function neural network for small rotary wing unmanned aircraft," *IEEE Trans. Indust. Electron.*, vol. 61, DOI 10.1109/TIE.2013.2289901, no. 9, pp. 4808-4815, Sept. 2014.

[18] N. H. Giap, J. H. Shin, and W. H. Kim, "Robust adaptive neural network control for XY table," *Intell. Contr. and Autom.*, vol. 4, DOI 10.4236/ica.2013.43034, no. 3, pp. 293-300, 2013.

[19] Y. Zou, and X. S. Lei, "A compound control method based on the adaptive neural network and sliding mode control for inertial stable platform," *Neurocomputing*, vol. 155, DOI 10.1016/j.neucom.2014.12.074, pp. 286– 294, May 2015.

Fei Dong was born in Shandong Province, China, in 1991. He received the B.S. degree in measurement and control technology and instrument from Shandong University, Jinan, Shandong Province, China, in 2014.Since then, he has been working toward the M.S. degree in instrument science and technology at Beihang University, Beijing, China.

His research interests include high performance control for inertial stabilized platform, and low cost SINS/GPS integrated navigation.

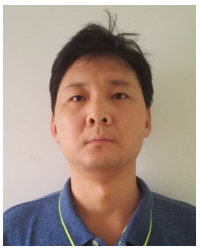

Xusheng Lei was born in Henan, China, in 1977.

He received the B.S. degree from Zhengzhou University, Zhengzhou, China, in 1998; the M.S. degree from Henan University of Science and Technology, Luoyang, China, in 2002; and the Ph.D. degree from Shanghai Jiaotong University, Shanghai, China, in 2006.

He is currently with the Science and Technology on Inertial Laboratory, School of Instrumentation Science and Optoelectronics Engineering, Beihang University, Beijing, China. His main research interests include high-performance control for small unmanned aerial vehicles and intelligent control for inertial stable platforms.

Wusheng Chou was born in Xinjiang, China, in 1969. He received the B.S. and M.S. degrees in electrical engineering from Tianjin University, Tianjin, China, in 1990 and 1995 respectively, and the Ph.D. degree in mechanical engineering from the same university, in 1998.

He is currently a Professor with the School of Mechanical Engineering and Automation, Beihang University, Beijing, China. His main research interests include industrial automation, embedded control and mechatronics.